Superalloys 2012: 12th International Symposium on Superalloys
Edited by: Eric S. Huron, Roger C. Reed, Mark C. Hardy, Michael J. Mills, Rick E. Montero, Pedro D. Portella, Jack Telesman
TMS (The Minerals, Metals & Materials Society), 2012

INFLUENCE OF RUTHENIUM ON TOPOLOGICALLY CLOSE PACKED PHASE PRECIPITATION IN SINGLE-CRYSTAL NI-BASED SUPERALLOYS: NUMERICAL EXPERIMENTS AND VALIDATION

R. Rettig and R.F. Singer
Institute of Science and Technology of Metals; University of Erlangen; Martensstr. 5; D-91058 Erlangen, Germany

Keywords: precipitation, modeling, CALPHAD, TCP-phases, ruthenium

Abstract

The suppression of topologically close-packed phases (TCP) in nickel-based single-crystal superalloys by the addition of ruthenium is modeled with a fully multicomponent mesoscale precipitation model based on the numerical Kampmann-Wagner-method using thermodynamic CALPHAD-calculations. For the application of the model in ruthenium-containing superalloys, mobility assessments of the binary systems nickel-ruthenium (Ni-Ru) and nickel-rhenium (Ni-Re) were performed to create a new mobility database. It is postulated that the dominating effect of ruthenium regarding more sluggish TCP-phase precipitation is a change of interface energy reducing the number of precipitates nucleating. The precipitation sequences occurring during TCP-phase precipitation can be explained using CALPHAD thermodynamics.

Introduction

Rhenium-containing single crystal superalloys have gained great interest in the last two decades due to their increased creep strength [1]. This leads to a considerable increase of the turbine blade operation temperature in stationary and aeroengine gas turbine applications. As efficiency is directly related to the turbine inlet temperature, the turbine efficiency is raised and emissions are decreased [2]. Besides the positive effects of Re on the deformation rate, it has been frequently reported that Re strongly decreases the alloy stability and promotes precipitation of brittle topologically close packed (TCP) phases [3-8]. TCP precipitation is highly undesirable and eventually limits the amount of Re that can be added to advantage: On the one hand Re, which preferentially enters the TCP-phases, is removed from the matrix [9, 10] lowering the solution strengthening effect, while on the other hand the brittle and needle-like precipitates may grow to considerable size where they act as crack initiation sites [6, 7, 10].

One promising solution is the addition of ruthenium to the alloy. It is now widely accepted that this element strongly decreases the susceptibility to TCP-phase precipitation after Re addition. Alloys containing rhenium and ruthenium show superior creep properties [11, 12]. Heckl et al. [13] concluded that with addition of 1 at-% Re the maximum application temperature can be increased by 87 K. Even an addition of 1 at-% Ru raises the limit by 38 K in low Re-containing alloys. Nevertheless concerns are rising due to the very high price of both elements, which requires careful optimization of the alloy composition [14].

The detailed mechanisms of the Ru-effect are still under dispute [9, 11, 15-19], because the experimental investigation of the retarded precipitation process is difficult and the alloy system is very complex. In the following, numerical simulation will be employed to shed some light on the Ru effect.

Numerical simulation

Thermodynamic modeling

The CALPHAD-method (Calculation of Phase Diagram) allows not only the calculation of phase diagrams, but the derivation of thermodynamic properties in general, like driving forces or phase compositions. The basic idea of the CALPHAD-method is the numerical determination of the phase compositions with minimum total Gibbs enthalpy in the system – i.e. the equilibrium state. For this purpose, the Gibbs free enthalpy of the different phases is modeled as the sum of the Gibbs free enthalpies of the chemical elements, the ideal and the non-ideal mixing enthalpy. Due to the latter term, the relation must be fitted to experimental results and those parameters are stored in thermodynamic databases. For further details on the CALPHAD-method, the reader is redirected to standard textbooks. In the present work, the ThermoCalc (version R) software interface TC-API (version 4, ThermoCalc, Stockholm, Sweden) was used together with the commercial thermodynamic database TTNi7 (ThermoTech Ltd, Surrey, UK) [20] for all CALPHAD-calculations.

Diffusion modeling

The diffusion in multicomponent systems (n elements including Ni) is described by the extended Fick's law, where $\vec{j}_k$ is the diffusion flux of element k, c_j is the concentration of the element j and $\tilde{D}_{kj}^{n}$ the matrix of the interdiffusion coefficients [21]. The distance is defined as x. The non-diagonal elements of this matrix are the so-called cross-diffusion coefficients.

$$\vec{j}_k = -\sum_{j=1}^{n-1} \tilde{D}_{kj}^{n} \frac{\partial c_j}{\partial x} \tag{1}$$

The multicomponent extension considers not only the gradient of the diffusing element k but of all elements.

It is more convenient to express diffusion with the diffusion mobilities M_i, as rather than (n-1)x(n-1) diffusion coefficients, only (n-1) mobilities have to be assessed. The intrinsic diffusion coefficient and the mobility are connected by a thermodynamic factor $\partial\mu_i / \partial x_j$, where x_j is the molar fraction of element j. Therefore, the intrinsic diffusion coefficient D_{kj}^{V} can be expressed as:

$$D_{kj}^{V} = \sum_{i=1}^{n} \left(\delta_{ik} - x_k\right) x_i M_i \frac{\partial \mu_i}{\partial x_j} \tag{2}$$

This describes the diffusion in the volume-fixed frame of reference and can be converted to the interdiffusion coefficient $\tilde{D}_{kj}^{n}$, which is obtained from diffusion experiments, as follows:

$$\tilde{D}_{kj}^{n} = D_{kj}^{V} - D_{kn}^{V} \tag{3}$$

δ_{ik} in eq. 2 is the Kronecker symbol. The mobilities M_i have to be assessed with respect to the dependency on composition and temperature and are stored in mobility databases. The mobility can be described by a Boltzmann-approach with the activation energy ΔQ_i and the frequency factor Θ_i, which depends on the lattice parameter a and the jump frequency ω of the atoms:

$$M_i = \frac{\Theta_i}{\mathrm{R}T} exp\left(-\frac{\Delta Q_i}{\mathrm{R}T}\right) \tag{4}$$

$$\Theta_i = a^2 \cdot \omega \tag{5}$$

Following other work, Θ_i is set to 1 because the absolute values of the parameters are of no importance. In this case the assessment of the mobilities can be reduced to the temperature and concentration dependency of ΔQ_i. In analogy to the classical CALPHAD-approach, this dependency is successfully modeled with a Redlich-Kister-polynomial. This allows assessing the model parameters Q_i^j and ${}^{k}A_i^{pj}$ with the same optimization software as used for thermodynamic database development:

$$\Delta Q_i = \sum_j x_j Q_i^j + \sum_p \sum_{j>p} x_p x_j \sum_k {}^{k}A_i^{pj} \left(x_p - x_j\right)^k \tag{6}$$

In analogy to [22], ${}^{0}A_i^{pj}$ is assumed to be constant and Q_i^j is modeled with a linear dependency on temperature:

$$Q_i^j = V_{i,A}^j + V_{i,B}^j \cdot T \tag{7}$$

The parameters $V_{Ni,A}^{Ni}$ and $V_{Ni,B}^{Ni}$ have to be consistent with existing data in other binary systems Ni-X in order to integrate them into one database. For all assessments, the software code DICTRA version 24 (ThermoCalc, Stockholm, Sweden) was used and the results were integrated into the existing database from [22]. In the simulations, the mobilities were again obtained from the database with the programming interface TC-API.

Precipitation kinetics modeling

Due to the availability of the CALPHAD-method with significant thermodynamic models, meaningful precipitation models can be developed even for complex multicomponent systems. The main challenge of these systems is that the composition at the interface between matrix and precipitate depends on a complex set of equations describing flux balances and thermodynamic equilibrium.

In the present work the fully multicomponent precipitation model developed in [23] was applied, which is based on the numerical Kampmann-Wagner-method. In general, use of the numerical Kampmann-Wagner method is an alternative to the phase-field method. Here, the Kampmann-Wagner method is chosen because long-term simulations with phase field over thousands of simulation hours in multicomponent systems are still very challenging due to the long computation times.

In the following, only a short overview of the multicomponent numerical Kampmann-Wagner method shall be presented; details on theory and implementation can be found in [23]. It was implemented using MATLAB 2007b (MathWorks, Ismaning, Germany). The basic idea is to group the precipitates into a number of classes; each contains all particles nucleated in a certain time step. All these particles share the same concentration and size. In each time step, nucleation and growth are considered separately (see figure 1). Based on the regularly updated nucleation rate, it is decided if a new precipitate class is formed in the time step. After this step, the current growth rate of the already existing precipitate classes is calculated with a fully multicomponent growth law. Next the matrix concentration is adapted, because the matrix is depleted due to the precipitation. This depletion causes a steady change of precipitation driving force as the system approaches equilibrium.

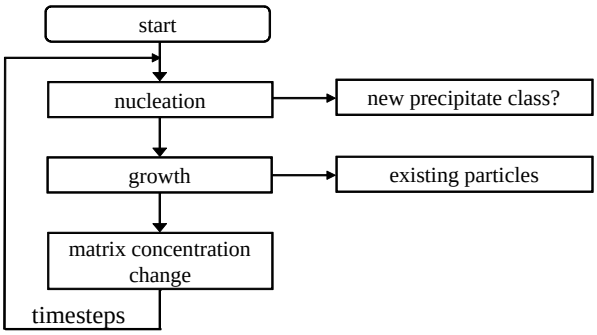

Figure 1. Basic algorithm of the mesoscale Kampmann-Wagner precipitation model.

The major model parameters are the energy of the interface between matrix and precipitate and the number density of available nucleation sites. The model is very sensitive to both. Number density can be estimated from metallographic analysis of the precipitates, but it must be considered that it is also depending on the driving force for precipitation [23]. The second parameter, the interface energy, cannot be determined directly by experimental methods. It is therefore most often gained from fitting experimental results to the precipitation model. Examples can be found in [24, 25] as well as in this work. As an alternative, calculations with ab-initio methods are emerging but these methods can still not be applied to complex multicomponent alloy systems without difficulties.

The precipitation model from [23] allows the time-dependent calculation of TTT-diagrams, driving forces, precipitate and matrix concentrations and the length of precipitates in complex alloy systems for single precipitate phases as well precipitation sequences.

Experiments

In the following, the results from the calculations will be compared to experiments, mostly taken from the work of our own research group, e.g. [10, 16, 26].

Typically, precipitation of needle-like TCP-phases with lengths of up to 50 µm or more is observed in the bulk. However, so called TCP-phase cell colonies with a comparatively coarse microstructure also can be found at large-angle grain boundaries.

The mechanism of formation is similar to the secondary reaction zone (SRZ) which is often observed beneath thermal barrier coatings [26]. Oversaturation of the γ-matrix as well as interface stresses cause a discontinuous transformation of the two-phase γ/γ'-microstructure into a cellular 3-phase structure with a γ'-matrix and lamellar γ- and TCP-phase precipitates. The reaction can be described as [26]:

$$\gamma(\text{matrix}) + \gamma'(\text{precip.}) \rightarrow \gamma'(\text{matrix}) + \gamma(\text{precip.}) + \text{TCP} \qquad (8)$$

The cell colony is growing away from the original grain boundary with a continuous reaction front. This type of phase transformation was mostly found in 3rd generation superalloys containing 6 wt-% Re.

An interesting aspect of the discontinuous transformation is that it allows for a reliable determination of TCP-phase fraction as well as phase composition in equilibrium, as it obviously represents the final stage of the phase transformation [26]. This is similar to eutectoid transformations in steels. Due to the large dimensions, the phase compositions can be easily measured with the microprobe (EPMA) method – transmission electron microscopy (TEM) is not required. Another advantage is the shorter time required for the reaction to occur compared to bulk discontinuous transformation. As such, in the present study cell colonies were used for obtaining the TCP-phase fraction as a function of the Ru-content of the alloy. The measured TCP-phase fractions were evaluated by image analysis from SEM-images.

Results

In this study all required properties and parameters for understanding the influence of Ru on TCP-phase precipitation using a fully multicomponent model are derived and verified systematically. At first kinetic and thermodynamic databases are developed, then the major parameters of precipitation (interface energy and nucleate density) are analyzed in a parameter study and the influence of ruthenium on the TCP-phase precipitation is investigated using the developed parameters. Finally the thermodynamics of the TCP-phase precipitation sequences are examined.

Mobility database for ruthenium-containing superalloys

An appropriate mobility database is required for precipitation modeling. In the field of nickel-based superalloys, a published database from [22] for the elements Ni–Al–Co–Cr–Hf–Mo–Re–Ta–Ti–W exists. It has been widely applied, but a reliable assessment of the mobilities in the system Ni-Ru is still missing.

Thus an assessment of the binary system Ni-Ru was performed, and due to the importance of rhenium in the presented model, the system Ni-Re was reassessed. The work of [22] and others proved that already by integrating mobility descriptions of the binary subsystems, it is possible to develop a reliable diffusion database. Both binary models were designed for incorporation into the existing database by choosing the model parameters for pure Ni identical to those of [22]. The assessments were performed with the experimental data given in table I and were based on the mobility model described in a previous section. Data at temperatures lower than 900 °C was not considered, because [22] raised concerns about grain boundary diffusion below that temperature. All required thermodynamic data was taken from the database [20].

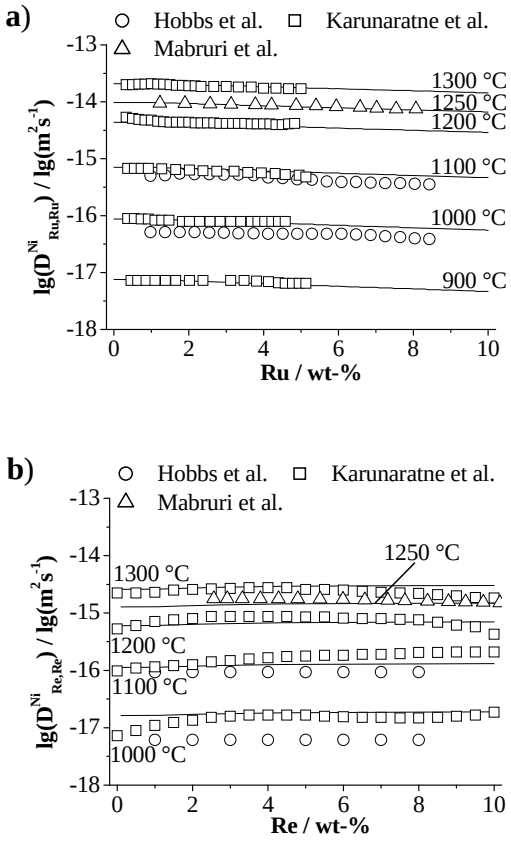

Figure 2. Assessment of the diffusion coefficients in the binary systems (a) Ni-Ru and (b) Ni-Re. The DICTRA-model (solid lines) is compared to the experimental data from [17, 27-29]. The datasets describe well all experiments.

The results of the assessments in the system Ni-Ru are presented in figure 2a and the assessed parameters are given in table II. This dataset is consistent and fits well to literature data from [17, 28, 29]. The derived model can reasonably be extended far into the metastable region with high ruthenium contents. This is a prerequisite for the application of the model in a multicomponent database.

The assessed dataset for the system Ni-Re also fits well to the experimental data (see figure 2b and table II). It fully confirms the assessment from [22].

Table I: Experimental data used for the assessment of the binary systems Ni-Re and Ni-Ru with estimated errors.

source	coeff.	error	conc.	temp. / °C	error
[30]	D^{*}_{Ni}	±10%	in Ni	876 – 1227	±5 °C
[17]	$\tilde{D}_{\mathrm{Re,Re}}^{\mathrm{Ni}}$	±10%	0 – 8 wt-%	1000 – 1100	±5 °C
[27]	$\tilde{D}_{\mathrm{Re,Re}}^{\mathrm{Ni}}$	±10%	0 – 10 wt-%	1000 – 1300	±5 °C
[29]	$\tilde{D}_{\mathrm{Re,Re}}^{\mathrm{Ni}}$	±20%	0 – 5 at-%	1250	±5 °C
[17]	$\tilde{D}_{\mathrm{Ru,Ru}}^{\mathrm{Ni}}$	±10%	0 – 8 wt-%	1000 – 1100	±5 °C
[28]	$\tilde{D}_{\mathrm{Ru,Ru}}^{\mathrm{Ni}}$	±10%	0 – 10 wt-%	900 – 1300	±5 °C
[29]	$\tilde{D}_{\mathrm{Ru,Ru}}^{\mathrm{Ni}}$	±20%	0 – 5 at-%	1250	±5 °C

Table II: Assessed parameters for diffusion mobility in the binary systems Ni-Re and Ni-Ru above 900 °C.

DICTRA-nomenclature	param.	value
rhenium		
MQ(FCC_A1&Re,Ni:VA)	Q_{Re}^{Ni}	-280864 – 101.4·T
MQ(FCC_A1&Re,Re:VA)	Q_{Re}^{Re}	-436000 – 71.2·T
MQ(FCC_A1&Re,Ni,Re:VA;0)	${}^{0}A_{Re}^{Ni,Re}$	218584
MQ(FCC_A1&Ni,Re:VA)	Q_{Ni}^{Re}	-436000 -71.2·T
MQ(FCC_A1&Ni,Ni,Re:VA;0)	${}^{0}A_{Ni}^{Ni,Re}$	-649914
ruthenium		
MQ(FCC_A1&Ru,Ni:VA)	Q_{Ru}^{Ni}	-303907 – 68.3·T
MQ(FCC_A1&Ru,Ru:VA)	Q_{Ru}^{Ru}	-294000 - 71.6·T
MQ(FCC_A1&Ru,Ni,Ru:VA;0)	${}^{0}A_{Ru}^{Ru,Ni}$	-107007
MQ(FCC_A1&Ni,Ru:VA)	Q_{Ni}^{Ru}	-294000 – 71.6·T
MQ(FCC_A1&Ni,Ni,Ru:VA;0)	${}^{0}A_{Ni}^{Ni,Ru}$	-70669

Modeling TCP-phase thermodynamics

In this section, the results of the thermodynamic calculations are verified and the influence of Ru is investigated. In a later section the study is extended towards the integrated modeling of precipitation kinetics and thermodynamics.

Equilibrium TCP phase fraction in a variety of alloys. At first, the thermodynamic modeling capabilities are evaluated in a general way. Results from the CALPHAD-calculation (database TTNi7 [20]) are compared with experimental observations in a large number of experimental alloys (EROS-alloys) reported previously by this research group (Volek et al. [10]). The composition range of the alloys investigated is given in Table III. Figure 3 shows the probability of finding experimentally TCP-phases versus a certain calculated TCP-phase fraction. The probability is defined as the ratio of alloys with TCP-phases detected compared to the total number of alloys investigated. For the evaluation, the alloys were grouped in dependence of the CALPHAD-calculated TCP-phase fraction. For example all alloys with 5 – 6 molar percent of TCP-phases are represented by the 6% data point. It is very clear from the diagram that there is a good correlation between a large TCP-phase fraction calculated with CALPHAD and the experimental observation of TCP-phases. This emphasizes the validity of the thermodynamic calculation approach. However, as will be shown below, kinetics must be considered, too.

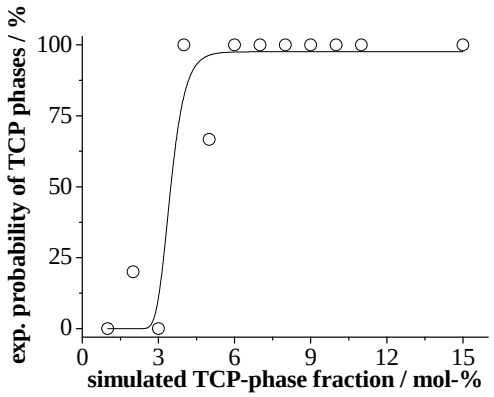

Figure 3. Correlation of the CALPHAD-simulated TCP-phase fraction and the probability of experimental observation of TCP-phases from Volek et al. [10] (exposure temperatures 750 – 980 °C and exposure times 500 – 5000 h). There is a clear correlation between simulated phase fraction and TCP-phase occurrence in the experiments.

Effect of Ru on TCP-phase fraction in equilibrium. The equilibrium TCP-phase fractions were taken from work published previously by our group [26]. The TCP-phase fraction in cell colonies was measured for different experimental ASTRA1-2x superalloys (x = 0, 1, 2 at-% Ru) as described above. The alloy compositions can be found in table III.

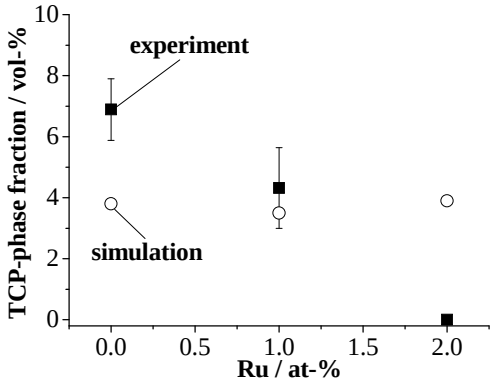

Figure 4. Measured equilibrium phase fraction of the TCP-phases in the ASTRA1-2x alloys (x = 0, 1, 2 at-% Ru) at 950 °C (experimental data: [26]) in comparison to calculations with CALPHAD (database: TTNi7). The phase fractions have been estimated from fast growing TCP-phase colonies at the grain boundaries. The equilibrium phase fraction is strongly reduced by addition of ruthenium.

The measured values are compared to thermodynamic equilibrium CALPHAD-predictions using the database TTNi7 (see figure 4). The experiments indicate a strong reduction of TCP-phase fraction with increasing Ru-content. In contrast to the experiments, the CALPHAD-calculations do not show any significant dependency.

A further finding in [26] was that the addition of 1 at-% Ru increased the average TCP-nuclei distance in the cell colony from 3.2 µm to 15.6 µm. This corresponds to a reduction of the nuclei density from $3 \cdot 10^{16}$ m^{-3} to $3 \cdot 10^{14}$ m^{-3}.

Modeling precipitation kinetics: Sensitivity study for interface energy and nuclei density

The sensitivity of the precipitation model [23] regarding its two major parameters is examined in order to prepare the calibration of the model. Interface energy and nuclei density are almost impossible to be determined experimentally. In figure 5 the influence of the nuclei density on the precipitation kinetics (a) and the interface energy on the TTT-diagram (b) is demonstrated.

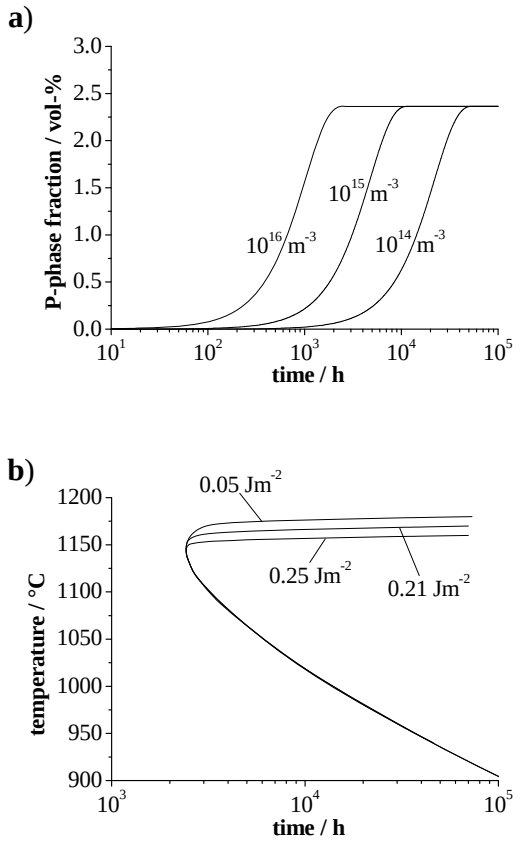

Figure 5. Sensitivity study on the influence of the major model parameters: (a) Nuclei density (phase fraction at 1100 °C) and (b) interface energy (TTT-diagram with 1 vol-% P-phase). Both calculations were performed for ASTRA1-20.

All other parameters remained unchanged and are documented in table IV. Both parameters investigated obviously have a strong impact. The nuclei density mostly influences the precipitate phase fraction at a certain time, while the interface energy has a strong influence on the temperature of maximum transformation rate ("nose temperature"). Comparing two alloys with different nucleate densities assuming otherwise unchanged growth conditions, the alloy with the larger nucleate density has a larger precipitate fraction after a certain time. The effect of interface energy can be explained in the following way: A larger value of interface energy increases the activation energy for nucleation thus requiring longer undercooling resulting in a lower nose temperature.

The nucleate densities N_0 and interface energies chosen in figure 5 are in a range which is typical for TCP-phase precipitates. The interface energies are in between those for coherent and semicoherent interfaces. The mean distance of the precipitates is given by $\sqrt[3]{1/N_0}$, which means that nucleate densities of 10^{16} m^{-3} and 10^{14} m^{-3} correspond to 4.6 µm and 21 µm, respectively.

Modeling precipitation kinetics: Ru-influence on the TCP-phase precipitation

The precipitation process is controlled by the thermodynamic driving force, by interface energy and diffusion rate. Ruthenium may influence all of them. The alloys TMS-121 (0 wt-% Ru), TMS-138 (2 wt-% Ru) and TMS-138+ (2.5 wt-% Ru, see table III) were chosen for the calculations because for them the TCP-phase precipitation including nucleation was already thoroughly investigated experimentally by Sato et al. [18, 19]. In these alloys, P-phase precipitation dominates. Sato et al. showed that Ru-additions have a strong impact on TCP-phase formation.

Table III. Composition of the alloys used in the present study. All values are given in wt-%. For the EROS-alloy series the minimum / maximum compositions are noted. The TMS-alloys contain additionally 0.1% Hf.

alloy	Al	Co	Cr	Mo	Re	Ru	Ta	W
EROS*	3.4 3.8	0.0 9.0	10 12	1.5 1.9	0.0 3.0	0.0 3.0	4.0	3.5
ASTRA1-20	5.9	8.6	5.0	0.9	6.0	-	6.4	5.9
ASTRA1-21	5.8	8.5	5.0	0.9	6.0	1.6	6.4	5.9
ASTRA1-22	5.8	8.4	5.0	0.9	5.9	3.2	6.3	5.9
TMS-121	6.0	6.0	3.0	3.0	5.0	-	5.7	6.0
TMS-138	5.9	5.9	2.9	2.9	4.9	2.0	5.6	5.9
TMS-138+	5.9	5.9	2.9	2.9	4.9	2.5	5.6	5.9

*additionally 0.08 wt-% C, 0.008 wt-% Zr

Figure 6 presents the driving force of P-phase precipitation calculated with the CALPHAD-method (database TTNi7). These results are later on used in the precipitation model. It is apparent that the driving force is decreasing with increasing temperature. There is only a small difference in the driving force for TCP-phase precipitation between the Ru-free and the Ru-containing

alloy. The difference is much too small to explain the strong reduction in TCP-precipitation with Ru-addition. This result is similar to the calculation of equilibrium phase fractions in the prior section (see figure 4). It is not clear at this point how to explain the discrepancy with the experiments. Either the CALPHAD-simulation underestimates the effect of Ru on the thermodynamic driving force or there is some other important effect of Ru.

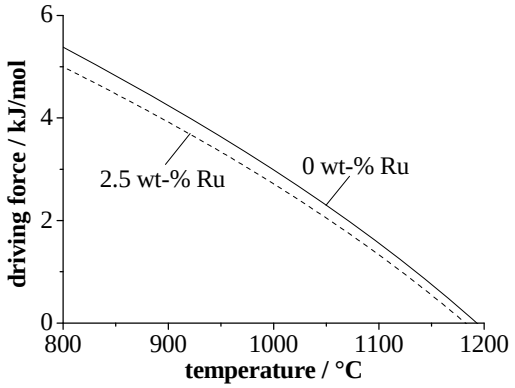

Figure 6. Thermodynamic (chemical) driving force of P-phase precipitation calculated with CALPHAD (database: TTNi7) in the alloys TMS-121 (0 wt-% Ru) and TMS-138+ (2.5 wt-% Ru) with differing ruthenium contents. The simulations indicate only a small difference, which cannot be confirmed by experiments.

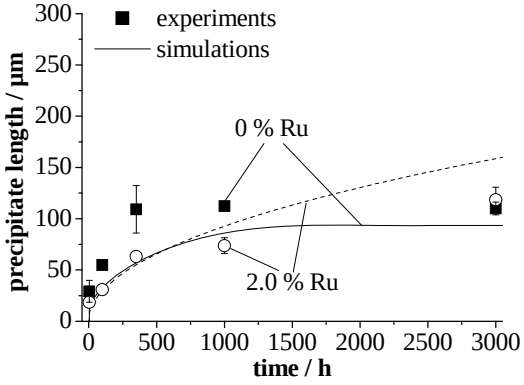

Figure 7. Calculated precipitate length as a function of annealing time at 1100 °C. The simulations are compared to experimental results from [19]. The precipitates in the alloy TMS-121 (0 wt-% Ru) are represented by closed points and a continuous line, while those in TMS-138 (2.0 wt-% Ru) are indicated by open points and the dashed line. The precipitates in the Ru-containing alloy have much larger interface energy.

Figure 7 shows the results for the final simulation of TCP-phase precipitation in alloys with different Ru-contents applying the model from [23]. They are compared to measurements from Sato et al. [18, 19]. The initial matrix concentration in the simulation is set to the estimated dendrite core composition (see table IV), because the TCP-phases occur mostly in this region, where the driving force is higher even after heat treatment due to residual segregation of Re and W. The segregation of all other elements can be neglected. Good agreement with Sato's results can be achieved with the nucleate densities and the interface energies given in table IV. All other required parameters are also noted there. The nucleate densities are consistent with the values which can be derived from the experimental work of Sato et al. ($3 \cdot 10^{15}$ m^{-3} without Ru and $9 \cdot 10^{13}$ m^{-3} with Ru). The experiments could only be matched reasonably if much larger interface energy is assumed for the Ru-containing alloy.

Modeling thermodynamics of precipitation sequence

Previously we assumed the type of TCP-phase precipitation to be known in advance. However, there are a multitude of phases and it is in general not simple to predict which TCP-phase will form. Additionally, complex precipitation sequences are common because metastable phases nucleate first due to coherent, i.e. low energy interfaces. The stepwise precipitation process then progresses towards energetically more stable phases with semi- or incoherent interfaces nucleating at the interface of the previously formed coherent phases.

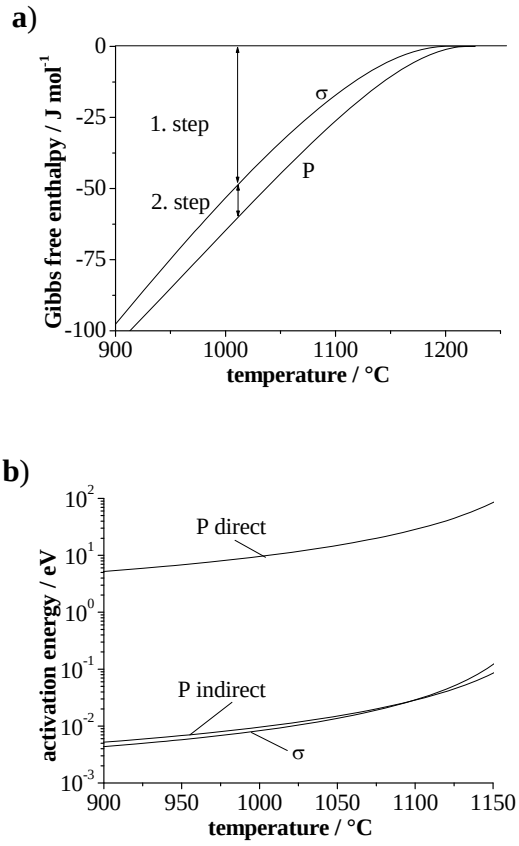

Figure 8. (a) Calculated Gibbs free enthalpy of the phases in the precipitation sequence of the TCP-phases and (b) activation energies for nucleation in the alloy ASTRA1-20. The indirect precipitation with the sigma phase as a metastable phase is energetically favorable.

The focus of the following is to show whether it is possible to predict precipitation sequences from CALPHAD-thermodynamics.

Figure 8a shows thermodynamic calculations of the Gibbs free enthalpy of the σ- and the P-phase in the alloy ASTRA1-20. The results clearly prove that the σ-phase has a significantly smaller Gibbs enthalpy and is therefore metastable compared to the P-phase. This means that from a thermodynamic point of view, the existence of precipitation sequences for TCP-phases can be rationalized and the σ-phase is expected to be the first phase to form (provided it features suitable low energy interfaces). This is in accordance with the experimental observations [5].

Additionally, the activation energy ΔG^* for σ- and P-phase nucleation in ASTRA1-20 has been calculated (see figure 8b) according to the relationship below, with γ being the interface energy, ΔG_v the CALPHAD-driving force, ΔG_s the misfit strain and f_{het} a factor considering heterogeneous nucleation:

$$\Delta G^* = \frac{16\pi\gamma^3}{3\left(\Delta G_v - \Delta G_s \cdot f_{het}\right)^2} \quad (9)$$

All required driving forces were taken from CALPHAD-calculations; the other parameters are noted in table IV. For simplicity the energy of a coherent interface is assumed to be 0.05 Jm^{-2} and 0.5 Jm^{-2} for an incoherent one. In accordance with the previously mentioned simple model of precipitation sequences and experimental observations from the work of Rae et al. [5], it is assumed that the σ-phase is coherent and the P-phase is incoherent in the case of nucleation in the bulk (direct precipitation). It is further assumed that the P-phase becomes coherent in case of nucleation at the interface of the existing σ-phase precipitates (indirect precipitation). Figure 8b shows that based on these simple assumptions dramatic differences in the calculated activation energy are obtained. Obviously the probability for the incoherent P phase to form directly in the bulk will be very low.

Table IV. Physical parameters of the precipitation model. Further details on the model parameters can be found in [23]. The other parameters are the activation energy of self-diffusion in the lattice ΔG_t = 255 kJ/mol, the strains due to lattice mismatch ε = 3.6% and the shear modulus G = 70 GPa. The heterogeneity factor is set to f_{het} = 0.2.

figure	nucleate density N_0 / m^{-3}	interface energy γ / Jm^{-2}	form factor Φ	alloy
fig. 5a	$1.0 \cdot 10^{14}$	0.05 (P)	200	ASTRA1-20
fig. 5a	$1.0 \cdot 10^{15}$	0.05 (P)	200	ASTRA1-20
fig. 5a	$1.0 \cdot 10^{16}$	0.05 (P)	200	ASTRA1-20
fig. 5b	$1.0 \cdot 10^{15}$	0.05 (P)	200	ASTRA1-20
fig. 5b	$1.0 \cdot 10^{15}$	0.21 (P)	200	ASTRA1-20
fig. 5b	$1.0 \cdot 10^{15}$	0.25 (P)	200	ASTRA1-20
fig. 7	$2.5 \cdot 10^{16}$	0.05 (P)	500	TMS-121*
fig. 7	$1.0 \cdot 10^{15}$	0.27 (P)	500	TMS-138*
fig. 8b	-	0.05 (σ)	-	ASTRA1-20
fig. 8b	-	0.5(σ, P)	-	ASTRA1-20

*The concentrations of Re and W are increased in the simulation by a factor of 1.5 respectively 1.05 compared to the nominal composition in order to model the incomplete homogenization in the dendrite core of the alloy. The calculations are thus representative for the dendrite core.

Discussion

Mechanism of suppression of TCP-phases by ruthenium

Precipitation can be separated into two processes, nucleation and growth. Ruthenium might affect both steps. The rate of transformation and resulting size distribution of the TCP-phase at a given time and temperature is controlled by:

1. nucleation rate (nuclei density, controlled by diffusion rate and activation energy barrier)
2. growth rate (speed of phase interface, controlled by diffusion rate and driving force)

Extending the ideas from Hobbs et al. [9], the influences of ruthenium regarding precipitation might be due to:

1. change in γ'-phase fraction
2. change in partitioning between γ- and γ'-phase (reverse partitioning)
3. change in interface energy between matrix and precipitate
4. change of diffusivity

The effect of Ru on the γ'-phase plays a major role because many TCP-phase forming elements like Re and W are hardly soluble in this phase and the matrix concentration of these elements depends on the γ'-phase composition and volume fraction.

Consequences of Ru addition

γ'-phase fraction and reverse partitioning. In the literature it is controversial as to whether Ru changes the γ'-phase fraction and the partitioning ratio of Re between γ- and γ'-phase. On the one hand, Hobbs et al. [9] observed a reduced γ'-fraction in the alloy SRR300D with 3 wt-% ruthenium addition compared to the same alloy without Ru. On the other hand Neumeier et al. [15] did not find a significant change in another experimental alloy. There is probably a dependence on the general alloy composition, explaining such different findings. Further, the error in the γ'-phase fraction measurements is comparatively large.

The influence of the ruthenium concentration on the γ/γ'-partitioning ratio has been debated for a long time and "reverse partitioning", which describes the intensified partitioning of rhenium into the γ'-phase upon addition of ruthenium, is often given as the only explanation for the ruthenium effect [15, 16, 31-34]. The many different results in literature for a large range of superalloy compositions let us conclude that the "reverse partitioning effect" is probably strongly dependent on the overall alloy composition. Carroll et al. [35] support this experimentally as well as our previous numerical study [36]. There is evidence that "reverse partitioning" only occurs if the chromium content is rather low.

The fundamental question is how a change of alloy characteristics may lead to decelerated TCP-phase precipitation. In earlier work of the same authors [36], the multicomponent model as used in the present study was applied in a numerical experiment addressing this question. In that study the γ'-phase fraction was reduced by 5 mol-% (approximately 5 vol-%) without changing any other features in the alloy. In a second experiment the partitioning ratio

of Re was reduced by one third keeping everything else constant. Both assumed changes in the alloy are very large and can be taken as upper limits for what seems likely. The numerical experiments showed that precipitation will be reduced, but the effect is very small compared to the Ru-effect observed in reality. Thus we conclude that a change of γ'-phase fraction and γ/γ'-partitioning ratio by addition of Ru are not the only reasons for the important Ru effect on TCP-phase precipitation.

Interface energy. The interface energy between matrix and TCP-phases can be estimated based on the calculations presented above (see figure 7 and table IV). The results indicate a large increase of the interface energy between matrix and precipitate with addition of Ru from 0.05 to 0.27 Jm^{-2}. It is very difficult to compare the values quantitatively with literature results because there is little relevant research. Robson et al. and Sourmail et al. found for example 0.25 – 0.33 Jm^{-2} for TCP- and Laves-phases in austenitic stainless steels [24, 37].

A reason for a change of interface energy with addition of Ru might be the segregation of Ru into the matrix / TCP-interface and thus a local change of the chemistry. Further high resolution observations have to be conducted in order to prove this hypothesis.

Diffusion rate. Hobbs et al. [17] and Mabruri et al. [29] have measured the dependence of the rhenium diffusion coefficient on the ruthenium content. They found that it is not at all influenced by ruthenium. As rhenium is the most important TCP-phase former, it seems that the growth rate, which is dependent on the diffusion coefficient, is not altered by ruthenium. In accordance with this, figure 7 shows only a moderate influence of ruthenium on the growth rate.

Influence of Ru on speed of transformation

The results in the present study are ambiguous as far as an influence of Ru on the thermodynamics is concerned, i.e. the driving force for precipitation of TCP-phases seems to be hardly affected. This suggests that the explanation for the reduced rate of TCP formation might be a change in nucleation rate caused by changes in interface energy. The activation energy for nucleation is controlled by driving force and interface energy. According to the discussion in the previous section, the addition of ruthenium probably increases the activation energy via an increase of interface energy. As such, in the ruthenium containing alloy, there are less active nucleation sites available, which means that less precipitates are formed and that the time to the identical precipitate fraction is longer, because individual precipitates have to grow larger. The experimental measurements of TCP-nucleate densities in alloys with different Ru-contents from Sato et al. [19] as well our group's work [26] clearly support this idea.

Precipitation sequences

The situation in case of TCP-phase precipitation is similar to precipitation in other alloy systems. The final equilibrium phases are incoherent or semicoherent while the first phases to form feature low energy boundaries. According to Rae et al. [5] the σ-phase exhibits crystal planes with an extraordinarily small misfit to the superalloy γ-matrix. They therefore postulate and experimentally prove that the σ-phase is the first metastable phase to be formed and later on the equilibrium TCP-phase, which can be μ- or P-phase depending on the alloy composition, is nucleated at the σ-interface rather than in the bulk in order to save surface energy. Our thermodynamic calculations support this interpretation because the σ-phase is a metastable phase in the investigated alloy. Additionally, it became evident that the stable P-phases (assuming high interface energy) have very large activation energy and can hardly nucleate directly.

Conclusions

1. A new mobility database for ruthenium containing superalloys was developed which describes the Ni-Ru system consistently.

2. Ruthenium affects the TCP-phase precipitation mostly by retarding nucleation. It is postulated that this is dominated by an increase of interface energy between matrix and TCP-phase on Ru-addition. The influence on reverse partitioning and γ'-phase fraction seems to be smaller.

3. The number of nuclei is strongly reduced by Ru due to larger activation energies, while the growth rate of the precipitates is essentially unchanged.

4. According to experimental results, Ru might increase the thermodynamic stability of the alloy regarding TCP-phase formation.

5. The σ-phase is metastable and therefore precipitation sequences of the TCP-phases are allowed by thermodynamics.

Acknowledgements

This work has received funds by the German Science Foundation (DFG) from the Research Training Group 1229/1 "Stable and Metastable Multiphase Systems for High Temperature Applications". John Ågren and Samuel Hallström (KTH Stockholm, Sweden) are gratefully acknowledged for support with the mobility assessments.

References

1. H. Harada, "High temperature materials for gas turbines: The present and future". In: *International Gas Turbine Congress*. Edited by M. Ito, T. Sakai, A. Tsuge, Tokyo, Japan, 2003, 1-9.

2. R.F. Singer, "Advanced materials and processes for land-based gas turbines", *Materials for Advanced Power Engineering*, 2 (1994), 1707-1729.

3. M. Pessah-Simonetti, P. Donnadieu, P. Caron, "TCP phase particles embedded in a superalloy matrix: Interpretation and prediction of the orientation relationships", *Scripta Metallurgica et Materialia*, 30 (1994), 1553-1558.

4. R. Darolia, D. Lahrman, R. Field, "Formation of topologically closed packed phases in nickel base single crystal superalloys". In: *Superalloys 1988*. Edited by S. Reichman, D. Duhl, G.

Maurer, S. Antolovich, C. Lund, Seven Springs, USA: The Metallurgical Society, 1988, 255-264.

5. C. Rae, R. Reed, "The precipitation of topologically close-packed phases in rhenium-containing superalloys", *Acta Materialia*, 49 (2001), 4113-4125.

6. M. Simonetti, P. Caron, "Role and behavior of μ phase during deformation of a Nickel-based single crystal superalloy", *Materials Science and Engineering A*, 254 (1998), 1-12.

7. R. Reed, D. Cox, C. Rae, "Damage accumulation during creep deformation of a single crystal superalloy at 1150 °C", *Materials Science and Engineering A*, 448 (2007), 88-96.

8. R.A. Hobbs, L. Zhang, C.M.F. Rae, S. Tin, "The effect of ruthenium on the intermediate to high temperature creep response on high-refractory content single crystal nickel-base superalloys", *Materials Science and Engineering A*, 489 (2008), 65-76.

9. R. Hobbs, L. Zhang, C. Rae, S. Tin, "Mechanisms of Topologically Close-Packed Phase Suppression in an Experimental Ruthenium-bearing single-crystal Nickel-base superalloy at 1100 °C", *Metallurgical and Materials Transactions A*, 39 (2008), 1014-1025.

10. A. Volek, R. Singer, R. Bürgel, J. Grossmann, Y. Wang, "Influence of topologically closed packed phase formation on creep rupture life of directionally solidified Nickel-base superalloys", *Metallurgical and Materials Transactions A*, 37A (2006), 405-410.

11. K. O'Hara, W. Walston, E. Ross, R. Darolia, "Nickel base superalloy and article", Patent No. 5.482.789, United States, 1996.

12. A.C. Yeh, C.M.F. Rae, S. Tin, "High temperature creep of Ru-bearing Ni-base single crystal superalloys". In: *Superalloys 2004*. Edited by K.A. Green, T.M. Pollock, H. Harada, *et al.*, Seven Springs, USA: TMS, 2004, 677-685.

13. A. Heckl, S. Neumeier, M. Göken, R.F. Singer, "The effect of Re and Ru on γ/γ' microstructure, γ-solid solution strengthening and creep strength in nickel-base superalloys", *Materials Science and Engineering A*, 528 (2011), 3435-3444.

14. M.V. Nathal, "NASA and superalloys: A customer, a participant, and a referee". In: *Superalloys 2008*. Edited by R.C. Reed, G. K.A., P. Caron, *et al.*, Seven Springs, USA: TMS, Warrendale, 2008, 13-19.

15. S. Neumeier, F. Pyczak, M. Göken, "The influence of ruthenium and rhenium on the local properties of the gamma- and gamma prime-phase in nickel-base superalloys and their consequences for alloy behavior". In: *Superalloys 2008*. Edited by R.C. Reed, K.A. Green, P. Caron, *et al.*, Seven Springs, USA: TMS, 2008, 109-119.

16. A. Volek, F. Pyczak, R.F. Singer, H. Mughrabi, "Partitioning of Re between gamma and gamma prime phase in Nickel-base superalloys", *Scripta Materialia*, 52 (2005), 141-145.

17. R.A. Hobbs, M.S.A. Karunaratne, S. Tin, R.C. Reed, C.M.F. Rae, "Uphill diffusion in ternary Ni-Re-Ru alloys at 1000 and 1100 °C", *Materials Science and Engineering A*, 460-461 (2007), 587-594.

18. A. Sato, Y. Koizumi, T. Kobayashi, T. Yokokawa, H. Harada, H. Imai, "TTT diagram for TCP phases precipitation of 4th generation Ni-base superalloys", *Journal of the Japan Institute of Metals*, 68 (2004), 507-510.

19. A. Sato, H. Harada, T. Yokokawa, T. Murakumo, Y. Koizumi, T. Kobayashi, *et al.*, "The effects of ruthenium on the phase stability of fourth generation Ni-base single crystal superalloys", *Scripta Materialia*, 54 (2006), 1679-1684.

20. N. Saunders, M. Fahrmann, C. Small, "The application of CALPHAD calculations to Ni-based superalloys". In: *Superalloys 2000*. Edited by K. Green, T. Pollock, R. Kissinger, Seven Springs, USA: TMS, 2000, 803-811.

21. J. Ågren, "Diffusion in phases with several components and sublattices", *Journal of Physics and Chemistry of Solids*, 43 (1982), 421-430.

22. C.E. Campbell, W.J. Boettinger, U.R. Kattner, "Development of a diffusion mobility database for Ni-base superalloys", *Acta Materialia*, 50 (2002), 775-792.

23. R. Rettig, R.F. Singer, "Numerical modelling of topologically close packed phase precipitation in nickel-based superalloys", *Acta Materialia*, 59 (2011), 317-327.

24. T. Sourmail, H.K.D.H. Bhadeshia, "Modelling simultaneous precipitation reactions in austenitic stainless steels", *CALPHAD*, 27 (2003), 169-175.

25. H. Sieurin, R. Sandström, "Sigma phase precipitation in duplex stainless steel 2205", *Materials Science and Engineering A*, 444 (2007), 271-276.

26. A. Heckl, S. Neumeier, S. Cenanovic, M. Göken, R.F. Singer, "Reasons for the enhanced phase stability of Ru-containing nickel-based superalloys", *Acta Materialia*, 59 (2011), 6563-6573.

27. M. Karunaratne, P. Carter, R. Reed, "Interdiffusion in the face-centred cubic phase of the Ni-Re, Ni-Ta and Ni-W systems between 900 and 1300 °C", *Materials Science and Engineering A*, 281 (2000), 229-233.

28. M. Karunaratne, R. Reed, "Interdiffusion of the platinum-group metals in nickel at elevated temperatures", *Acta Materialia*, 51 (2003), 2905-2919.

29. E. Mabruri, S. Sakurai, Y. Murata, T. Koyama, M. Morinaga, "Diffusion and gamma prime phase coarsening kinetics in ruthenium containing nickel based alloys", *Materials Transactions*, 49 (2008), 792-799.

30. B. Jönsson, "Assessment of the mobilites of Cr, Fe and Ni in fcc Cr-Fe-Ni alloys", *Zeitschrift für Metallkunde*, 86 (1995), 686-692.

31. S. Tin, A.C. Yeh, A.P. Ofori, R.C. Reed, S.S. Babu, M.K. Miller, "Atomic partitioning of ruthenium in Ni-based superalloys". In: *Superalloys*. Edited by K.A. Green, T.M. Pollock, H. Harada, *et al.*, Seven Springs, USA: TMS, 2004, 735-741.

32. S. Tin, L. Zhang, G. Brewster, M. Miller, "Investigation of Oxidation Characteristics and Atomic Partitioning in Platinum and Ruthenium Bearing Single-Crystal Ni-Based Superalloys", *Metallurgical and Materials Transactions A*, 37A (2006), 1389-1396.

33. T. Yokokawa, M. Osawa, K. Nishida, T. Kobayashi, Y. Koizumi, H. Harada, "Partitioning behavior of platinum group metals on the gamma and gamma prime phases of Ni-base superalloys at high temperatures", *Scripta Materialia*, 49 (2003), 1041-1046.

34. R.C. Reed, A.C. Yeh, S. Tin, S.S. Babu, M.K. Miller, "Identification of the partitioning characteristics of ruthenium in single crystal superalloys using atom probe tomography", *Scripta Materialia*, 51 (2004), 327-331.

35. L. Carroll, Q. Feng, J. Mansfield, T. Pollock, "High refractory, low misfit Ru-containing single-crystal superalloys", *Metallurgical and Materials Transactions A*, 37A (2006), 2927-2938.

36. R. Rettig, A. Heckl, R.F. Singer, "Modeling of precipitation kinetics of TCP-phases in single crystal nickel-base superalloys", *Advanced Materials Research*, 278 (2011), 180-185.

37. J.D. Robson, H.K.D.H. Bhadeshia, "Modelling precipitation sequences in power plant steels. Part 2 - Application of kinetic theory", *Materials Science and Technology*, 13 (1997), 640-644.